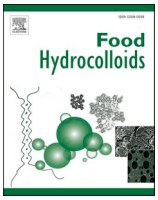
Food Hydrocolloids 178 (2026) 112681



Contents lists available at ScienceDirect

Food Hydrocolloids

journal homepage: www.elsevier.com/locate/foodhyd





Interfacial and foam-stabilizing properties of Mung bean and Pigeon pea proteins obtained from wet conventional extraction

Ployfon Boonkor [a], Jasper Landman [a], Chaiwut Gamonpilas [b], Leonard M.C. Sagis [a,*]

[a] Laboratory of Physics and Physical Chemistry of Foods, Wageningen University, Bornse Weilanden 9, 6708WG, Wageningen, the Netherlands
[b] Advanced Polymer Technology Research Group, National Metals and Materials Technology Centre, National Science and Technology Development Agency, Pathum Thani, 12120, Thailand

ARTICLE INFO

Keywords:
Pulses
Mung bean
Pigeon pea
Interfacial rheology
Foaming properties
Air-water interface

ABSTRACT

Pulses are rich sources of protein (18–30%), and their proteins are potential sources for plant-based food applications. In this work, we focus on protein extracts from mung beans (MB) (*Vigna radiata*) and pigeon peas (PP) (*Cajanus cajan*), two sources widely cultivated in Asia, Africa, and Latin America. Both pulses were fractionated using a wet conventional extraction to obtain globulin-rich (GB) and albumin-rich (AB) fractions. We investigated the interfacial properties at the air-water interface (including adsorption kinetics, dilatational and surface shear rheology) and foaming properties of the individual albumin and globulin fractions for both pulses. The smaller particle size (4–5 nm) and lower surface charge (−9 mV) of AB fractions contributed to faster adsorption at air-water interfaces, resulting in around twofold higher foam overrun than their GB fractions. In both dilatational and surface shear rheology tests, MB-AB formed the stiffest and most brittle interfacial structure compared to other samples. On the other hand, PP-AB formed the least stiff and most stretchable interfacial structure. In surface shear frequency sweeps, PP-AB-stabilized interfaces showed a strong frequency dependence, displaying multimode Maxwell behavior, whereas all other fractions showed power law behavior (i.e., $G_i' \sim \omega^n$). PP-AB appeared to stabilize the air-water interface through the Marangoni effect rather than through imparting high elasticity to its interfacial film. Among GB fractions, the PP-GB-stabilized interface had stronger in-plane protein network interactions and notably higher resistance to density changes than that of MB-GB. These specific interfacial properties of PP-GB resulted in the highest foam stability among all samples, with a foam half-life time of ~200 min. MB proteins showed poor foam stability with foam half-life time of 50–60 min, and no significant differences were observed between its two protein fractions. Overall, PP proteins exhibited better foaming properties compared to MB proteins at the studied concentration (0.1%w/w). This study revealed that PP proteins show promising techno-functionality and can be potentially used in food applications.

1. Introduction

Foam is an important food structure. Many foods have an aerated structure, such as milk foams, meringues, mousses, and cakes. Foams in food products typically consist of air bubbles (or carbon dioxide) dispersed in water and they are thermodynamically unstable (Walstra, 2003). To obtain stable foams, surfactants are required to lower interfacial tension and help prevent bubble coalescence (Walstra, 2003). Proteins, owing to their amphiphilic nature, are commonly used to stabilize the air-water interface in foam-based foods, especially those derived from animal sources (e.g., caseins, bovine serum albumin and lysozyme) (Ho et al., 2022; Ismail et al., 2020; Zhao et al., 2021).

Over the past few years, plant-based foods gained substantial attention, driven by increasing consumer awareness of sustainability, food security, health and well-being, and the need for diversified protein sources (Prakash et al., 2023). Pulses, the edible dry seeds of leguminous plants (e.g., peas, chickpeas, and lentils), are an important source used as functional ingredients in plant-based products. Generally, pulse seeds consist of 18–30% proteins and 50–65% carbohydrates, and they are low in fat (Chibbar et al., 2010). Besides the nutritional perspective, pulse proteins possess several techno-functional properties such as emulsion and foam stabilizing and the ability to form gels, making them suitable for a wide range of food applications (Boye et al., 2010; Etzbach et al., 2024). Globulins and albumins are major proteins found in pulses.

* Corresponding author.
E-mail address: leonard.sagis@wur.nl (L.M.C. Sagis).

https://doi.org/10.1016/j.foodhyd.2026.112681
Received 9 December 2025; Received in revised form 25 February 2026; Accepted 16 March 2026
Available online 17 March 2026
0268-005X/© 2026 The Authors. Published by Elsevier Ltd. This is an open access article under the CC BY license (http://creativecommons.org/licenses/by/4.0/).

Globulins, the storage proteins, account for approximately 70–80% of the total protein content in pulses (Tripathi et al., 2021). The dominant globulins in pulses are vicilins and legumins and they are oligomeric proteins. Legumins are typically organized as hexametric assemblies comprising six subunits which interact through noncovalent interactions, with a molecular weight (Mw) ranging from 300 to 400 kDa. Vicilins are trimers and have Mw ranging from 145 to 190 kDa (Tripathi et al., 2021). Albumins are water-soluble proteins with a Mw ranging between 5 kDa and 80 kDa. They also contain enzymatic proteins, protease and amylase inhibitors, and lectins (Boye et al., 2010).

Mung bean and pigeon pea are two commercially important pulse crops in many countries. Mung beans (MB) (*Vigna radiata L.*) short-duration legumes adapted to warm-season cultivation are important agricultural crops across many Asian countries (Pratap et al., 2021). MB seeds are a rich source of protein with a protein content of 21%–31% and they are low in fat (1.2%–1.6%) (Anwar et al., 2007). Pigeon peas (PP) (*Cajanus cajan* L.) are drought-tolerant pulses that originated from Asia, Africa, and South America (Locali-Pereira et al., 2023). PP seeds consist of 15.5 to 28.8% protein content, depending on various factors such as genetic variant and environmental conditions (Oomah et al., 2011). Like other pulses, the major protein of MB and PP are globulins. In MB, an 8S-vicilin type dominates their globulin fraction (89%) while the predominant globulin in PP is of the 7S-vicilin type (Mendoza et al., 2001; Oomah et al., 2011). Several previous studies have reported promising techno-functionality of MB proteins (Brishti et al., 2017; Du et al., 2018; Huang et al., 2024; Li et al., 2010; Yang et al., 2023; Yi-Shen et al., 2018) and PP proteins (Oshodi & Ekperigin, 1989; Syed et al., 2022; Tang et al., 2021).

However, the relationship between molecular structure, interfacial properties, and protein functionality of these pulse proteins is still poorly known compared to animal-derived proteins or other plant-based proteins. To design and formulate new plant-based products efficiently, knowledge relevant to these relations is important. In addition, systematic comparison of interfacial and functional properties of their different protein fractions (i.e., globulins and albumins) remains limited, particularly in PP proteins. In this study, we focus on foaming properties which are particularly relevant for the development of aerated food products. Specifically, our aim was to establish the link between physicochemical properties of the individual albumin and globulin fractions of mung bean and pigeon pea, and their interfacial rheological and foam stabilizing properties. The pulse proteins were fractionated using wet conventional extraction to obtain globulin-rich and albumin-rich fractions. We study interfacial properties of these pulse proteins at air-water interfaces including adsorption kinetics, linear and nonlinear dilatational and shear rheology, and systematically link the results of these tests to their techno-functionality (i.e. foamability and foam stability) comparing the two types of pulses and their individual protein fractions.

2. Materials and methods

2.1. Materials

Peeled mung beans (MB) were purchased from Raitip (Thailand). Peeled pigeon peas (PP) were purchased from Suanpana (Thailand). Sodium phosphate monobasic monohydrate and sodium phosphate dibasic anhydrous were purchased from VWR International (OH, USA). All solutions were prepared in ultrapure water (MilliQ Purelab Ultra, Darmstadt, Germany).

2.2. Wet conventional extraction

Dry peeled MB and PP seeds were milled into flour using a Multimill Hosokawa System (Hosokawa Micron B·V., Doetinchem, the Netherlands). Subsequently, the MB and PP flour was used for protein extraction by a wet conventional method following Chutinara et al. (2024). MB and PP flour was dispersed in MQ water at a 1:10 (w/v) ratio. The mixture was adjusted to pH 9.0 ± 0.05 by 1M NaOH and continuously stirred for 1.5 h at room temperature. After that, the dispersion was centrifuged at 13,000×*g* for 15 min. The supernatant was collected and adjusted to pH 4.6 ± 0.05 by 1M HCl for 30 min for achieving protein precipitation, followed by centrifugation at 13,000×*g* for 15 min. Both pellet and supernatant were collected in this step.

The supernatant containing soluble proteins (albumins) was dialyzed at 4 °C, using a 3–5 kDa cut off membrane (Spectrum Laboratories, Inc., Rancho Dominguez, CA, USA) against demi-water. The dialysate was exchanged at least 4 times until the conductivity was lower than 10 μS/cm. After dialysis, the sample was filtered through filter paper (Whatman No. 1, Sigma-Aldrich, USA) and the pH was adjusted to pH 7.0 ± 0.05 by 1M NaOH. The sample was then freeze-dried by Laboratory freeze dryers (Christ Freeze dryer Alpha 2–4 LD plus) to obtain an albumin-rich fraction (AB).

The pellet which mainly contained globulins was washed twice with MQ water and re-dispersed in MQ water at a ratio of 1:10 (w/v). The dispersion was adjusted the pH to 7.0 ± 0.05 by 1M NaOH and stirred for 2 h. After that, the sample was dialyzed using the same method mentioned above, but the membrane size was changed to a 12-14 kDa cut-off. After dialysis, the sample was freeze-dried by Laboratory freeze dryers (Christ Freeze dryer Alpha 2–4 LD plus) to obtain a globulin-rich fraction (GB). All freeze-dried samples were stored at −18 °C prior the further experiments.

2.3. Protein content

An amount of 3–5 mg of pulse protein was weighed, and its nitrogen content was determined using the Dumas technique (FlashSmart, ThermoScientific, USA) at least in triplicate. The protein content was then calculated using a nitrogen-to-protein conversion factor of 5.7 (Yang et al., 2022).

2.4. Protein solubility

A 1% (w/w) of protein dispersion was prepared in phosphate buffer (20 mM, pH7) and stirred continuously for 3 h. The solution was kept at 4 °C overnight to allow complete hydration of the protein. The protein solution was then filtered using 0.22 μm filters. The protein solubility was measured by determining the protein content of the filtrate after drying in an oven at 60 °C using Dumas (FlashSmart, ThermoScientific, USA) (Shen et al., 2024).

2.5. Protein dispersion preparation

Protein dispersions for subsequent measurements were prepared following the method of protein solubility (Sec. 2.4) at 0.1% (w/w) based on the soluble protein content as determined by Dumas, unless otherwise specified. The particle size experiments were conducted at 0.01% (w/w) protein concentration by successive dilutions of 0.1% (w/w) protein dispersions.

2.6. Size exclusion chromatography (SEC)

Size exclusion chromatography was performed using an ÄKTA pure system equipped with a UV detector and Superdex 200 increase 10/300 GL column. A protein dispersion (1% w/w) was prepared using phosphate buffer (20 mM, pH 7) containing 150 mM NaCl and then filtrated with a 0.45 μm filter. Subsequently, the filtrate (50 μL) was injected into the SEC system with the same phosphate buffer as the eluent and the flow rate was 0.75 mL/min. Protein composition was analyzed with a UV wavelength at 214 nm (Shen et al., 2024). The measurements were conducted in duplicate.

2.7. Particle size and zeta potential

The particle size distribution and zeta-potential were determined using a Zetasizer (Nano ZS, Malvern Instruments, UK) using dynamic light scattering. The particle size and zeta-potential were measured at protein concentrations of 0.01%w/w and 0.1%w/w, respectively. These measurements were conducted at least in duplicate. The refractive indices of proteins and water phases were set to 1.45 and 1.33, respectively.

2.8. Surface hydrophobicity

The surface hydrophobicity was determined using 8-anilino-1-naphthalenesulfonic acid ammonium salt (ANSA) as a fluorescence agent, according to Chutinara et al. (2024). Protein dispersions were prepared in a phosphate buffer (20 mM, pH 7) with a protein concentration in the range of 0.005 – 0.04% (w/w). The protein solution (3 mL) was mixed with 8 mM ANSA solution (25 μL) and incubated for 1 h in a dark place. Afterward, the measurement was carried out using a spectro-fluorophotometer (RF6000, Shimadzu, Japan) with an excitation wavelength of 390 nm, and an emission wavelength set at 470 nm. The slope of the fluorescence intensity versus protein concentration was used as a quantification of the surface hydrophobicity. The measurement was conducted in duplicate.

2.9. Adsorption behavior and surface dilatational rheology at air-water interfaces

The adsorption behavior and surface dilatational rheology were determined using an automated drop tensiometer TRACKER™ (TECLIS Instruments, France). A rising air bubble with an area of 12 mm^2 was generated at the tip of a u-shape needle, immersed into a cuvette filled with 5 mL protein dispersion 0.1% (w/w). The surface tension was determined by bubble profile analysis and calculated based on the Young-Laplace equation by the built-in software. The results were expressed in terms of surface pressure, defined as $\Pi = \gamma_{aw} - \gamma(t)$ (where γ_{aw} is the surface tension of the clean air-water interface and $\gamma(t)$ is the measured surface tension). After 3 h of adsorption, surface dilatational rheology was performed including frequency sweeps and amplitude sweeps. In frequency sweeps, the frequency was increased from 0.005 Hz to 0.1 Hz at an amplitude of 3%, which was in linear viscoelastic region (LVE) for all samples (Shen et al., 2024). In the amplitude sweeps, the amplitude was increased from 1% to 60% at a fixed frequency of 0.02 Hz. All experiments were carried out at 20 °C and at least in triplicate.

To study the responses in the linear and nonlinear viscoelastic regime of the pulse protein-stabilized interfaces, Lissajous (LJ) plots were generated by plotting oscillating surface pressure ($\Pi(t) = \gamma(t) - \gamma_0$) against time dependent deformation ($= (A(t) - A_0)/A_0$). Here γ_0 and A_0 are the surface tension and area of the undeformed interface while $\gamma(t)$ and $A(t)$ are the surface tension and area of the deformed interface at time t. LJ plots were further analyzed using the general stress decomposition (GSD), to further interpret and quantify the asymmetric responses in the nonlinear regime (de Groot et al., 2023; Pivard et al., 2024).

2.10. Surface shear rheology

Surface shear rheology was conducted using a MCR302e rheometer (Anton Paar, Austria) with a double wall ring (DWR) geometry. An amount of 15 mL of protein dispersion (0.1% w/w) was filled into a cylindrical Teflon trough, and then the DWR geometry was lowered and positioned at the air-water interface, followed by pre-shearing at 0.1 s^{-1} for 2 min. A solvent trap was used to prevent liquid evaporation. The proteins were allowed to adsorb to the interface for 3 h without disturbing. After that, the interface was subjected to shear oscillations. Frequency sweeps were performed at a fixed strain of 1% and frequency was increased from 0.01 Hz to 10 Hz. Strain sweeps were conducted by increasing strain from 0.1% to 100% at a fixed frequency of 1 Hz. The experiments were performed in triplicate at 20 °C. To study rheological properties in the nonlinear regime, Lissajous (LJ) plots were constructed from surface shear stress as a function of strain during sinusoidal oscillation. The energy dissipation ratio (Φ) was further calculated according to Ewoldt et al. (2008).

2.11. Microstructure of the air-water interface

Langmuir-Blodgett (LB) films at air-water interfaces were prepared using a Langmuir trough (KSV NIMA/Biolin Scientific Oy, Finland). To prepare the film, phosphate buffer (20 mM, pH 7) was filled into the Teflon trough and a mica sheet was immersed in the buffer. A platinum Wilhelmy plate was used to monitor the surface pressure. Protein dispersion (0.1%w/w) was injected at the bottom of the trough followed by allowing the protein to adsorb without disturbing for 3 h. After that, the two barriers were moved (at a speed of 5 mm/min) to compress the protein layers until reaching a surface pressure of 13 mN/m or 23 mN/m. Then, the mica sheet was lifted from the solution (at a constant speed of 1 mm/min) to deposit the interfacial film onto the mica sheet. All LB films were kept in a desiccator for at least one day prior to further experiments. The experiment was performed in duplicate at room temperature.

Atomic force microscopy (AFM, NanoWizard® 4XP, NanoScience, Bruker Nano GmbH, Germany) with a PEAKFORCE-HIRS-FA cantilever (Bruker Nano GmbH, Germany) was used to visualize the protein structure at the air-water interface, following the method of Shen et al. (2024). All LB films were imaged and then processed by the built-in JPK data processing software (Bruker Nano GmbH, Germany). To quantitatively characterize the interfacial structure, AngioTool 64 (National cancer Institute, National Institute of Health, Maryland, USA) was used to performed image analysis according to (Bernklau et al., 2016; Shen et al., 2024); Zudaire et al. (2011). Protein network analysis from AngioTool software gave as the following parameters: vessel area, total number of junctions, junction density, total vessel length, average vessel length, number of end points, and lacunarity.

2.12. Foaming properties of pulse proteins

The foaming properties of pulse proteins were studied using a whipping method. A 0.1% (w/w) protein dispersion was whipped by an aerolatte frother for 2 min at 2000 rpm in a glass cylinder. The percent overrun of each protein sample was determined by the foam volume (mL) divided by the initial liquid volume (mL) times 100 (Yang et al., 2022). Additionally, the foam stability of the pulse proteins (0.1% w/w) was evaluated using a sparging techniques in a Foamscan (TECLIS Instruments, France). The gas was sparged through a sintered glass frit (pore size 16–40 μm) with a gas flow rate of 100 mL/min. The time that half of the foam collapsed was considered as the half-life time, which was determined using a built-in camera of the Foamscan. The experiments were conducted at least in duplicate at 20 °C.

2.13. Statistical analysis

SPSS Statistics 30.0.0.0 software (IBM SPSS Inc. Chicago, USA) was used to perform statistical analysis using one-way ANOVA (analysis of variance) with Duncan's Post-Hoc test at $p < 0.05$.

3. Results and discussion

3.1. Properties and molecular composition of pulse protein extracts

Pulse proteins were obtained from wet conventional extraction, which included alkaline-solubilization followed by isoelectric point

precipitation. This technique allowed proteins to be separated into a globulin-rich fraction (GB) and albumin-rich fraction (AB). The protein composition and their properties were summarized in Table 1. Protein contents of MB-GB and PP-GB were 80% and 78%, respectively, suggesting high protein purity. AB fractions typically contain soluble proteins and other non-proteinaceous compounds such as fibers, starch and phenols, and therefore their protein purity was much lower compared to GB (48% and 61% for MB-AB and PP-AB, respectively). All pulse protein extracts showed high solubility with values higher than 85%.

The particle size of pulse proteins was determined using dynamic light scattering (Table 1). The particle size of the GB fractions was significantly larger than their AB fractions (~12 nm *vs* ~5 nm), and there were no significant differences between the studied pulse types. In addition, the zeta-potential of the fractions was determined, and GB fractions had approximately twice as negative values than the AB fractions at pH 7.0. Surface hydrophobicity is one of the important factors affecting surface properties of proteins which affects protein adsorption and intermolecular interactions between proteins at the interface (Phillips et al., 1994). MB-GB (1.0) possessed the highest relative surface hydrophobicity, followed by PP-GB (0.84), MB-AB (0.35) and PP-AB (0.30), respectively, and the surface hydrophobicity of GB fractions was ~35% higher than that of AB fractions. Our results corresponded with previous studies that GB of pulses (mung bean, lentil and faba bean) had higher surface hydrophobicity than their AB fractions (Shen et al., 2025; Yang et al., 2023).

Size exclusion chromatography (SEC) was performed to study the molecular distribution of pulse protein extracts as presented in Fig. 1. From SEC chromatograms of GB fractions, they mainly contained vicilin and legumin globulins. The major globulin found in MB was reported to be 8S-vicilin type with molecular weight (Mw) approximately 200 kDa (Huang et al., 2024; Mendoza et al., 2001; Yi-Shen et al., 2018). On the other hand, PP-GB was dominated by a 7S-vicilin type and was reported to have Mw of 184 kDa (Krishna & Bhatia, 1985; Locali-Pereira et al., 2025). Pulse legumins generally exhibit a hexamer form and have Mw approximately 300–400 kDa (Tripathi et al., 2021). In our study, the Mw of PP-vicilin was larger compared to MB-vicilin (207 kDa Vs 177 kDa). In addition, legumins of MB and PP showed Mw of 475 kDa and 661 kDa, respectively, which were larger than expected. This was possibly due to protein aggregation during sample preparation, hence not all of the legumins may have been in their native forms. The ratios of vicilin/legumin of MB-GB and PP-GB were calculated which were 2.8 and 1.5, respectively. In AB factions, the majority species of MB-AB and PP-AB were 21 kDa and 15 kDa, respectively. Small peaks in both MB-AB and PP-AB at elution volume around 12 mL were also observed, suggesting minor contamination by vicilins.

3.2. Adsorption behavior of pulse proteins-stabilized at air-water interfaces

The adsorption curves of the pulse proteins at air-water interfaces are shown in Fig. 2A and Fig. S1. In the initial adsorption stages, AB fractions from both MB and PP proteins increased surface pressure faster than their GB fractions. This was expected since the particle size of AB fractions (~4–5 nm) was smaller compared to GB fractions (~11–12 nm), resulting in faster adsorption. Additionally, AB fractions had a smaller molecular weight and lower surface charge than their GB fractions which contributed to a lower energy barrier for adsorption (Yang et al., 2023). At 5s – 100s, PP-AB displayed a significantly faster increase in surface pressure than MB-AB. This may possibly be due to PP-AB having a smaller molecular weight compared to that of MB-AB, leading to a faster diffusion toward the air-water interface (15 kDa Vs 21 kDa, Fig. 1). For the GB fractions, MB-GB showed slightly higher surface pressure at 1s compared to PP-GB. This could be related to MB-GB possessing higher relative surface hydrophobicity than PP-GB. At 3 h of adsorption, MB-GB, PP-GB, MB-AB and PP-AB increased surface pressure to 25.03 (±0.33) mN/m, 25.28 (±0.39) mN/m, 26.33 (±0.85) mN/m and 26.54 (±0.39) mN/m, respectively.

Adsorption curves for proteins are often analyzed in terms of multistage models, featuring an initially fast adsorption phase where the rate determining step is the diffusion of proteins towards the interface (alternatively, the adsorption can be energy-barrier limited). The structure formed by plant-based proteins then tends to reach an arrested state (typically within the first minute of adsorption; Shen et al., 2025), after which adsorption is much slower and is dominated by rearrangements of the adsorb proteins within the interface (see for example: Beverung et al. (1999); Rodríguez Patino et al. (2008)). Rearrangements can involve the partial denaturation of proteins and/or simple aging of the arrested state (detachment and reattachment of parts of the interfacial microstructure). Here, for the first 50s of adsorption, the surface pressure was plotted as a function of the square root of time (Fig. 2B). A straight line in such a plot would indicate that the adsorption would be in the diffusion-limited regime. We clearly see that all four samples, and particularly the albumin ones, have already passed this regime, and adsorption has entered the slow aging phase. To examine the nature of this aging state, frequency and amplitude sweeps were performed, which are discussed in the next section.

3.3. Dilatational rheology of pulse proteins-stabilized at air-water interfaces

After allowing protein adsorption for 3 h, oscillatory dilatational rheology measurements, including frequency and amplitude sweeps, were subsequently performed.

The frequency sweeps were performed in the linear viscoelastic (LVE) regime to gain more insight into the type of structure formed by all four protein fractions. In frequency sweeps, all pulse protein-stabilized air-water interfaces showed low frequency dependence in the studied frequency range, and fitting the response with a power law ($E_d' \sim \omega^n$) gave n-values in the range of 0.09 – 0.18 (Fig. 2C). The Lucassen and Van Den Tempel (1972) model predicts an n-value of 0.5, when the elasticity is dominated by diffusive exchange of stabilizers between the interface and bulk phase. In our samples, n-values were much lower than 0.5, which suggested low exchangeability of proteins between interface and bulk phase. The low values for n, together with the observation that $E_d' > E_d''$ over the entire tested frequency range indicates that the interface is in a disordered viscoelastic solid state and is either in a 2d gel or in a 2d soft glassy state.

Food products are often subjected to high stresses and strains during

Table 1
Pulse proteins composition and properties obtained from wet conventional extraction: protein content (%), solubility (%), average particle size (nm), zeta-potential (mV), and relative surface hydrophobicity (H_0).

Fraction	Protein content (%)	Solubility (%)	Average particle size (nm)	Zeta-potential (mV)	H_0
MB-GB	80.07 ± 0.70^{a}	97.34 ± 0.20^{a}	11.48 ± 3.32^{a}	-18.34 ± 2.91^{a}	1.00 ± 0.04^{a}
MB-AB	47.98 ± 3.78^{c}	92.68 ± 0.36^{c}	4.35 ± 1.51^{b}	-9.80 ± 1.63^{b}	0.35 ± 0.01^{c}
PP-GB	78.35 ± 1.16^{a}	86.09 ± 0.41^{d}	11.96 ± 2.54^{a}	-20.18 ± 2.80^{a}	0.84 ± 0.03^{b}
PP-AB	61.15 ± 3.54^{b}	96.08 ± 1.00^{b}	4.91 ± 1.12^{b}	-8.03 ± 1.16^{b}	0.30 ± 0.01^{d}

Mean value in the same column with different letters are significantly different ($p < 0.05$); MB-GB: mung bean globulin-rich fraction, MB-AB: mung bean albumin-rich fraction, PP-GB: pigeon pea globulin-rich fraction, and PP-AB: pigeon pea albumin-rich fraction.

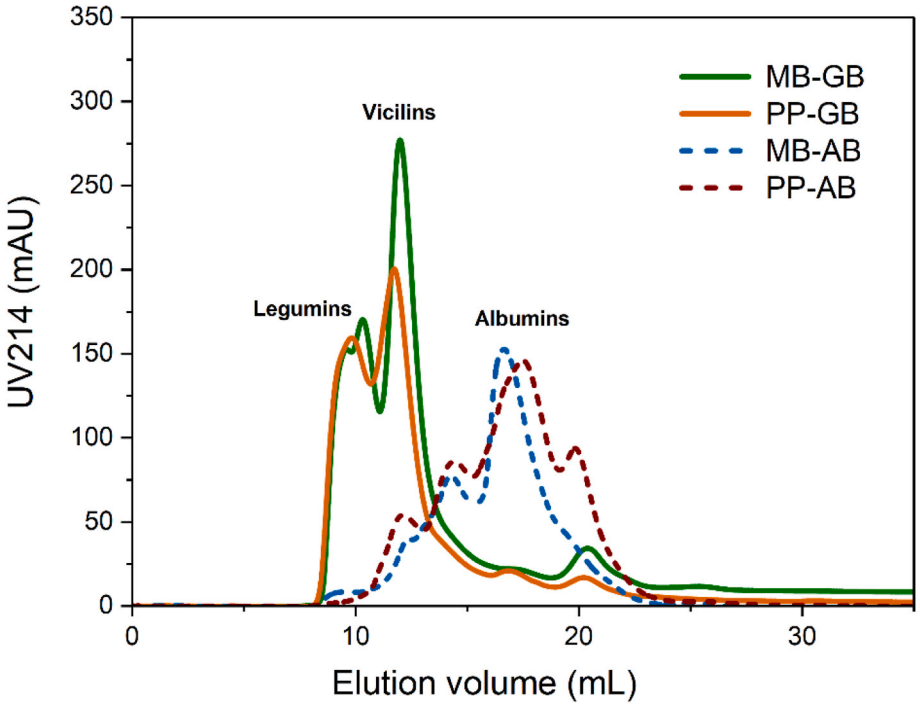


Fig. 1. Size exclusion chromatogram of pulse proteins as a function of elution volume at 214 nm UV absorbance. MB-GB (green), PP-GB (orange), MB-AB (blue), and PP-AB (red).

industrial and oral processing, and therefore it is also highly relevant to study the behavior of the interface in the nonlinear viscoelastic region (NLVE) (Joyner, 2021; Sagis & Yang, 2022). To obtain comprehensive results, we performed amplitude sweep in both the LVE and NLVE regions with deformation ranging from 1% to 60%. This will allow for determining the extend of the LVE regime, and the extent of disruption of the interfacial microstructure at large strains.

In amplitude sweeps, pulse protein-stabilized interfaces had higher values of the interfacial dilatational storage moduli (E_d') than their dilatational loss (E_d'') moduli (Fig. 2D). Over the entire applied strain range, and together with the low frequency dependence, this suggests disordered viscoelastic solid-like interfacial films were formed. At low deformation (1%), MB-AB-stabilized interfaces showed the highest E_d' (~67 mN/m) indicating the highest interfacial stiffness among all samples. The result was in line with previous finding that AB fractions from pulses (mung bean, lentil, fava bean, chickpea, and Bambara groundnut) were reported to display higher E_d' compared to their GB fractions (Shen et al., 2025; Yang et al., 2022, 2023). Typically, AB fractions have a smaller particle size and lower surface charge, generally facilitating stronger in-plane interaction between proteins and the formation of a denser structure at air-water interfaces. MB-GB and PP-GB showed similar dilatational moduli throughout the studied deformation range. At low deformation, their E_d' values were both lower than MB-AB. The GB fractions tend to have larger particle size and higher surface charge than AB fractions, which can lead to weaker protein-protein interactions and a less dense interfacial microstructure. When increasing deformation to 60%, the E_d' of all samples decreased by 47% – 73% which indicated the (partial) disruption of their interfacial microstructures. The E_d' of MB-AB decreased to the highest extent, which indicates its stiffer structure is also more brittle. Surprisingly, PP-AB behaved differently from other AB samples. The PP-AB-stabilized interface showed the lowest E_d' and the longest linear viscoelastic (LVE) region. This result was unexpected since PP-AB had similar physico-chemical properties (e.g., particle size and surface charge) to MB-AB, and this observed interfacial behavior is not typically found in pulse albumins. The PP-AB-stabilized interface appears to have the weakest protein in-plane interactions, resulting in the lowest stiffness and a highly stretchable interfacial film (i.e., with a long LVE regime).

The microstructure of pulse protein-stabilized interfaces is (partially) disrupted when applying large deformations. This results in nonlinear responses in which higher order harmonics emerge in the surface stress response of the interface (Sagis & Fischer, 2014). To better understand the mechanical properties of these pulse protein-stabilized interfaces in the nonlinear viscoelastic regime (NLVE), Lissajous (LJ) plots were constructed by plotting the oscillatory surface pressure against intra-cycle deformation. We constructed LJ plots from 5% to 40% deformation to compare the responses of these pulse protein-stabilized interfaces when deformation amplitude increases (Fig. 3). The part of the LJ plot to the right of the vertical axis demonstrates the extended state of the interface, and the part on the left side represents the compressed state of the interface.

At 5% deformation, LJ plots for all samples showed narrow ellipsoidal shapes which indicated a linear viscoelastic behavior with a dominant elastic component. When increasing the deformation amplitude, the LJ plots became wider, and more asymmetric shapes were observed. This suggested a nonlinear behavior and an increase in the contribution of the viscous components in the response of the protein-stabilized interfaces. At 40% deformation, strain softening was notably present in the extension phase of the cycle of all samples, as can be seen by a gradual decrease of the slope of the curve to almost zero at the end of the extension phase (upper right corner of the loop). The disruption of interfacial structures and the decrease in protein density at the interface is possibly associated with this strain softening phenomenon (Shen et al., 2024). In addition, strain-hardening was observed as a gradual increase in slope in the compression state, which could be related to an increase in protein density leading to a jamming of the interfacial structures (Shen et al., 2024). The MB-AB-stabilized interface showed the most pronounced changes in its LJ plots from 5% to 40%. At 40% deformation, the shape of the MB-AB plots showed the widest loop, indicating a higher dissipated energy compared to the other samples. In contrast, the LJ plots of PP-AB did not prominently change when deformation increased, as the plots remain much narrower compared to the other samples. This confirms the highly stretchable structure of the PP-AB-stabilized interface (Fig. 2D). We did not observe a major

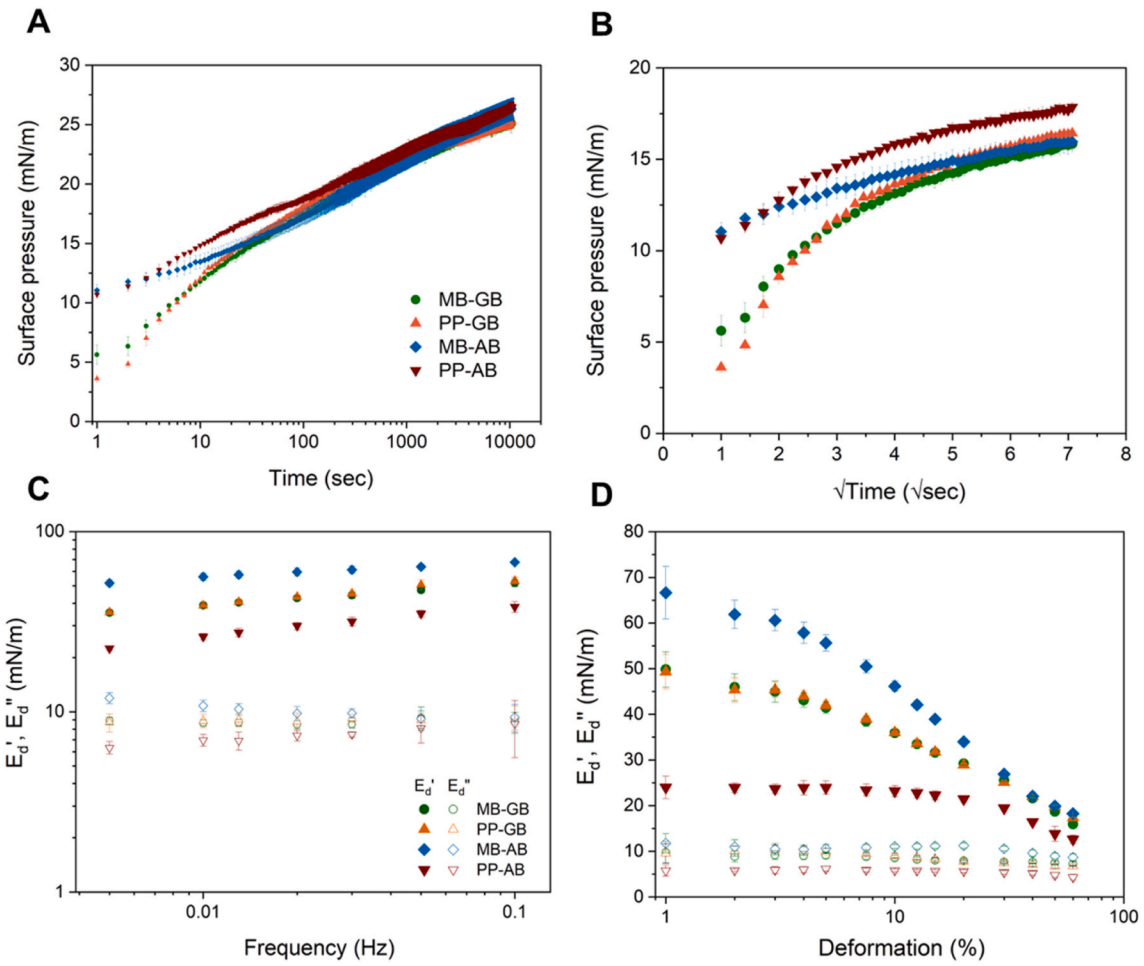


Fig. 2. **(A)** Surface pressure of pulse proteins at 0.1% (w/w) as a function of time; **(B)** Surface pressure of pulse proteins at 0.1% (w/w) as a function of the square root of time; **(C)** Interfacial dilatational storage (E_d') and loss (E_d'') moduli as a function of frequency, at a fixed amplitude of 3%. **(D)** E_d' and E_d'' as a function of deformation, at a fixed frequency of 0.02 Hz of pulse protein-stabilized air-water interfaces in phosphate buffer (20 mM, pH 7). Solid symbols represent E_d' and open symbols represent E_d''. MB-GB (green), PP-GB (orange), MB-AB- (blue), and PP-AB (red).

difference in LJ plots between the GB fractions. To further quantify the asymmetric responses of these pulse protein-stabilized interfaces, the LJ plots were decomposed in contributions from odd and even harmonics, and we will discuss these in the following section.

3.4. General stress decomposition (GSD) of lissajous plots

At large deformation, an asymmetry between the compression and extension phase in LJ plots can be observed (Sagis & Fischer, 2014). To gain more insightful and quantitative information from the LJ plots in the NLVE regime, the LJ plots were further analyzed using the general stress decomposition (GSD), following the method of de Groot et al. (2023) (Fig. 4 and Fig. S2). The original LJ plots at 40% deformation were decomposed into four components (i.e., $\tau1$, $\tau2$, $\tau3$ and $\tau4$). The stresses $\tau1$ and $\tau2$ represent the elastic and viscous contributions, respectively, from the odd harmonics in the Fourier spectrum, and are related to interfacial microstructure (i.e., network) disruptions. The stresses $\tau3$ and $\tau4$ represent the dissipative and reversible contributions, respectively, from even harmonics, which are related to contributions to the total stress induced by surface density changes (de Groot et al., 2023). These account for the nonlinearity of the surface equation of state. As an illustration, the decomposed plots at 40% deformation are shown in the SI (Fig. S2).

From these decomposed plots, we determined several quantitative parameters (Fig. 4). We determined $E_{\tau1L}$, the secant modulus of $\tau1$, which is the slope of the curve connecting the origin with the stress at maximum extension, and it quantifies interfacial network stiffness (de Groot et al., 2023). At increased deformation, the $E_{\tau1L}$ of these pulse protein-stabilized interfaces decreased, which demonstrated the occurrence of network disruption (Fig. 4A). The MB-AB-stabilized interface had the highest $E_{\tau1L}$ values (60 mN/m, at 3% deformation), and its $E_{\tau1L}$ decreased abruptly with increased deformation, suggesting it has stronger network interactions compared to the other samples. In addition, the MB-AB-stabilized interface had the highest dissipated energy, determined from the $\tau2$ contribution ($U_{d\tau2}$) (Fig. 4D). This could be due to the higher viscosity of its remaining structure after (partial) network disruption (de Groot et al., 2023). In contrast, the PP-AB-stabilized interface showed the lowest $E_{\tau1L}$ values (22 mN/m, at 3% deformation) and its $E_{\tau1L}$ only slightly decreased at higher deformation (Fig. 4A). Its value of $U_{d\tau2}$ also was significantly lower compared to all other samples, indicating a lower viscous contribution to the overall surface stress (Fig. 4D). Based on these results, PP-AB appears to have very weak in-plane interactions at the air-water interface. When comparing the GB fractions, MB-GB and PP-GB showed similar $E_{\tau1L}$ and $U_{d\tau2}$ values throughout the studied deformation (Fig. 4A and D).

Based on the contributions of $\tau3$ and $\tau4$, $E_{\tau4}$ is the secant modulus of $\tau4$, representing the resistance against surface density changes, while $U_{d\tau3}$ represents the area of the $\tau3$ loop, measuring the dissipated energy involved in surface density changes (de Groot et al., 2023). The $E_{\tau4}$ moduli of all pulse proteins decreased (i.e., became more negative) with

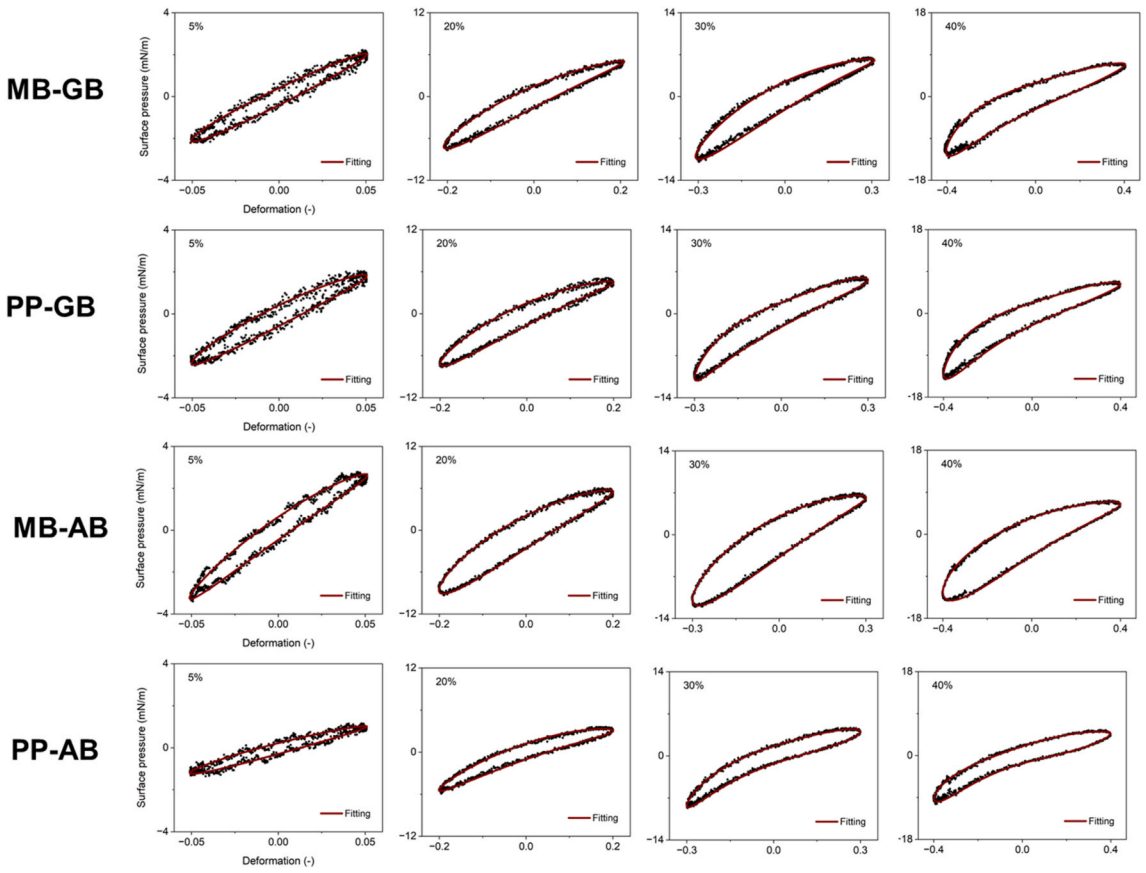


Fig. 3. Lissajous plots of surface pressure as a function of deformation obtained during amplitude sweeps at 5%, 20%, 30% and 40% deformation of pulse protein-stabilized air-water interfaces at a fixed frequency of 0.02 Hz. Y-axis shows surface pressure (mN/m) and X-axis shows deformation (−).

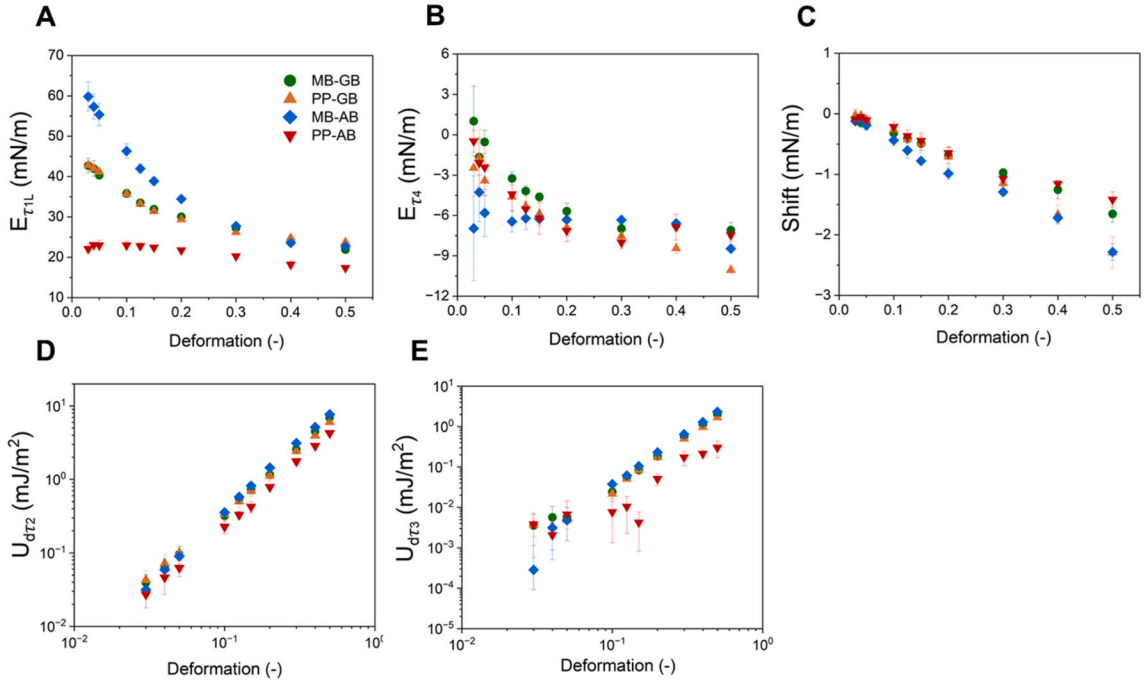


Fig. 4. Parameters determined from the stress decomposition of the Lissajous plots. The modulus $E_{\tau 1L}$ (**A**), modulus $E_{\tau 4}$ (**B**), vertical shift (γ_s) (**C**), the dissipated energy $U_{d\tau 2}$ (**D**), and the dissipated energy $U_{d\tau 3}$ (**E**) of MB-GB- (green), PP-GB- (orange), MB-AB- (blue) and PP-AB (red)-stabilized air-water interfaces, at a fixed frequency of 0.02 Hz.

increased deformation (Fig. 4B). This suggests a contribution of surface density changes due to (partial) irreversible adsorption of proteins.

Despite the similarity in τ1 and τ2 contributions, the $E_{\tau 4}$ of the PP-GB-stabilized interface had a much more negative value than that of MB-GB, at 50% deformation (Fig. 4B). This result implied a more limited exchangeability between bulk and interface and a higher resistance to density changes of the PP-GB-stabilized interface. The vertical shift of τ4 (γ_s) is a parameter measuring how far the system is driven out of equilibrium by the deformations. The γ_s of all pulse protein-stabilized interfaces became more negative when deformation increased (Fig. 4C). At 50% deformation, PP-GB and MB-AB-stabilized interfaces showed the most negative value of γ_s, implying that their interfaces cannot rapidly recover to a state of equilibrium at zero deformation due to the limited mobility of proteins (Ma et al., 2024). The PP-AB-stabilized interface had the least negative value of γ_s and the lowest values of $U_{d\tau 3}$ which confirmed the formation of a weak interfacial structure at the air-water interface (Fig. 4C and E).

3.5. Interfacial shear rheology

Interfacial shear rheology was used to further study the rheological properties of the interfaces stabilized by the four fractions. Unlike dilatational rheology, which induces area changes of surface elements while keeping the shape fixed, this technique changes the shape of surface elements while keeping the surface area constant (Sagis & Yang, 2022). Therefore, it tends to be more sensitive to in-plane network interactions, and stresses do not include contributions from density changes. After adsorption for 3 h, interfacial shear rheology was performed including frequency and amplitude sweeps. In the frequency sweeps, pulse proteins-stabilized interfaces had a low frequency dependence, and fitting the curves for the surface shear storage modulus G_i' with a power law ($G_i' \sim \omega^m$) gave m-values in the range of 0.15 – 0.19, except for the PP-AB-stabilized interface (Fig. 5A). The interface formed by PP-AB exhibited a behavior distinctly different from other samples, a difference which was even more pronounced than in dilatational rheology. It showed a high frequency dependence and a cross-over between G_i' and G_i'' (the surface shear loss modulus) was observed at a frequency of 0.01 Hz; this behavior resembles that of a (multi-mode) Maxwell fluid. This confirms our earlier observation from the dilatational rheology, that PP-AB has weak in-plane interactions at the air-water interface.

In amplitude sweeps, the G_i' of all pulse protein-stabilized interfaces showed higher values than G_i'' in the linear viscoelastic regime (Fig. 5B). This confirmed that these pulse proteins showed solid-like behavior at the applied frequency and small strains. At 0.01% – 1% deformation, the MB-AB-stabilized interface had the highest G_i' (~12 mN/m), indicating the strongest protein-protein in-plane interaction among all samples. In dilatational deformations, the interfacial network stiffness ($E_{\tau 1L}$) of both GB proteins showed similar values (Fig. 4A). In shear, we can see a difference between interfaces between the GB proteins, as PP-GB showed higher values for G_i' than MB-GB. This suggested that PP-GB has stronger in-plane network interactions. Just as in dilatation, where it had the lowest $E_{\tau 1L}$ values, the PP-AB-stabilized interface exhibited the lowest G_i' values and this confirmed that it had weak network interactions. From the combined results of dilatational and shear rheology, PP-AB appears to form a highly flexible and weak interfacial structure at the air-water interface. The fact that it shows a cross-over in the frequency sweeps at 0.01 Hz, means that at timescales longer than ~100 s, the microstructure of this interface is highly mobile and shows liquid-like behavior, and in foams (for which stability evolves over longer timescales). PP-AB possibly stabilizes the air-water interface through Marangoni effects rather than through imparting high stiffness to its interfacial film.

We also constructed LJ plots of surface shear stress versus intracycle strain (Fig. S3) and calculated the energy dissipation ratio (Φ) from these LJ plots (Fig. 5C). At low deformation (0.01% – 0.1%), the shear stresses for all pulse protein-stabilized interfaces were dominated by elastic behavior as their Φ values were in the range of 0.01 – 0.05. The Φ values of all interfaces gradually increased with increased deformation and reached values of 0.5 – 0.7 at 100% deformation. This indicated an increase of the viscous contribution as the interfacial network structures were (partially) disrupted. Comparing the GB fractions in the non-linear regime, the PP-GB-stabilized interface showed larger values for Φ than MB-GB, which suggested that PP-GB formed a stiffer and less stretchable interfacial structure. Interestingly, the Φ values of the PP-AB-stabilized interface showed an abrupt increase around 0.1% deformation while the MB-AB-stabilized interface showed a more gradual increase up to around 10% deformation, after which it increased to values close to PP-AB at 100%. The PP-AB-stabilized interface had the highest values of Φ at 100% deformation (0.7) among all samples. The results suggest that PP-AB tended to be more sensitive to shear deformation than dilatational deformation. Overall, we observed distinct interfacial properties of these pulse protein-stabilized interfaces. This suggests that they may have formed different interfacial structures at the air-water interface, which will be discussed in the following section.

3.6. Pulse protein-formed interfacial structures at air-water interface

To study the interfacial structures formed by the four pulse protein fractions at air-water interfaces, Langmuir-Blodgett films were prepared at a surface pressure of 23 mN/m which was close to the surface pressure after 3h of adsorption. After that the prepared films were imaged by AFM (Fig. 6). The AFM images were further analyzed with AngioTool image analysis software to obtain the protein network characteristics. In the AFM images, the bright areas represent the protein-rich regions. We found that all four pulse protein fractions formed heterogenous structures. Comparing the GB fractions at 23 mN/m, the MB-GB-stabilized interface had significantly higher vessels area and junctions density,

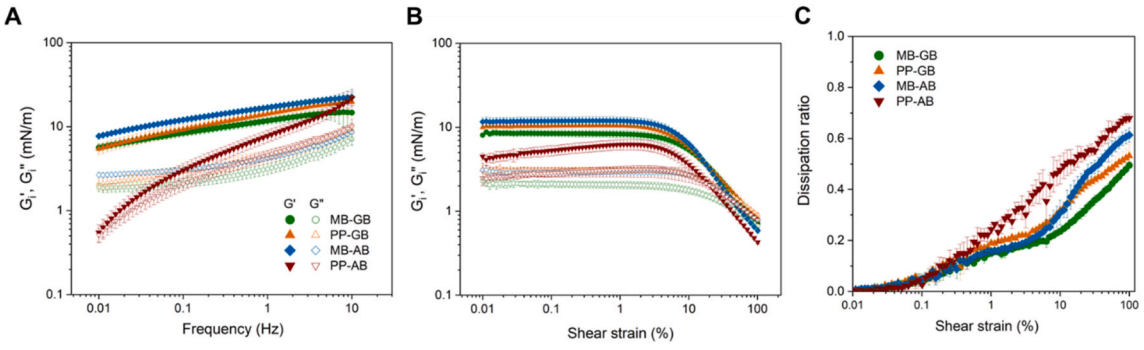


Fig. 5. **(A)** Interfacial shear storage (G_i') and loss (G_i'') moduli as a function of frequency, at a fixed strain of 1%. **(B)** G_i' and G_i'' as a function of shear strain, at a fixed frequency of 0.1 Hz of pulse protein-stabilized air-water interfaces in phosphate buffer (20 mM, pH 7). Solid symbols represent G_i', and open symbols represent G_i''. **(C)** The energy dissipation ratio (Φ) as a function of shear strain of pulse protein-stabilized interfaces. MB-GB (green), PP-GB (orange), MB-AB (blue), and PP-AB (red).

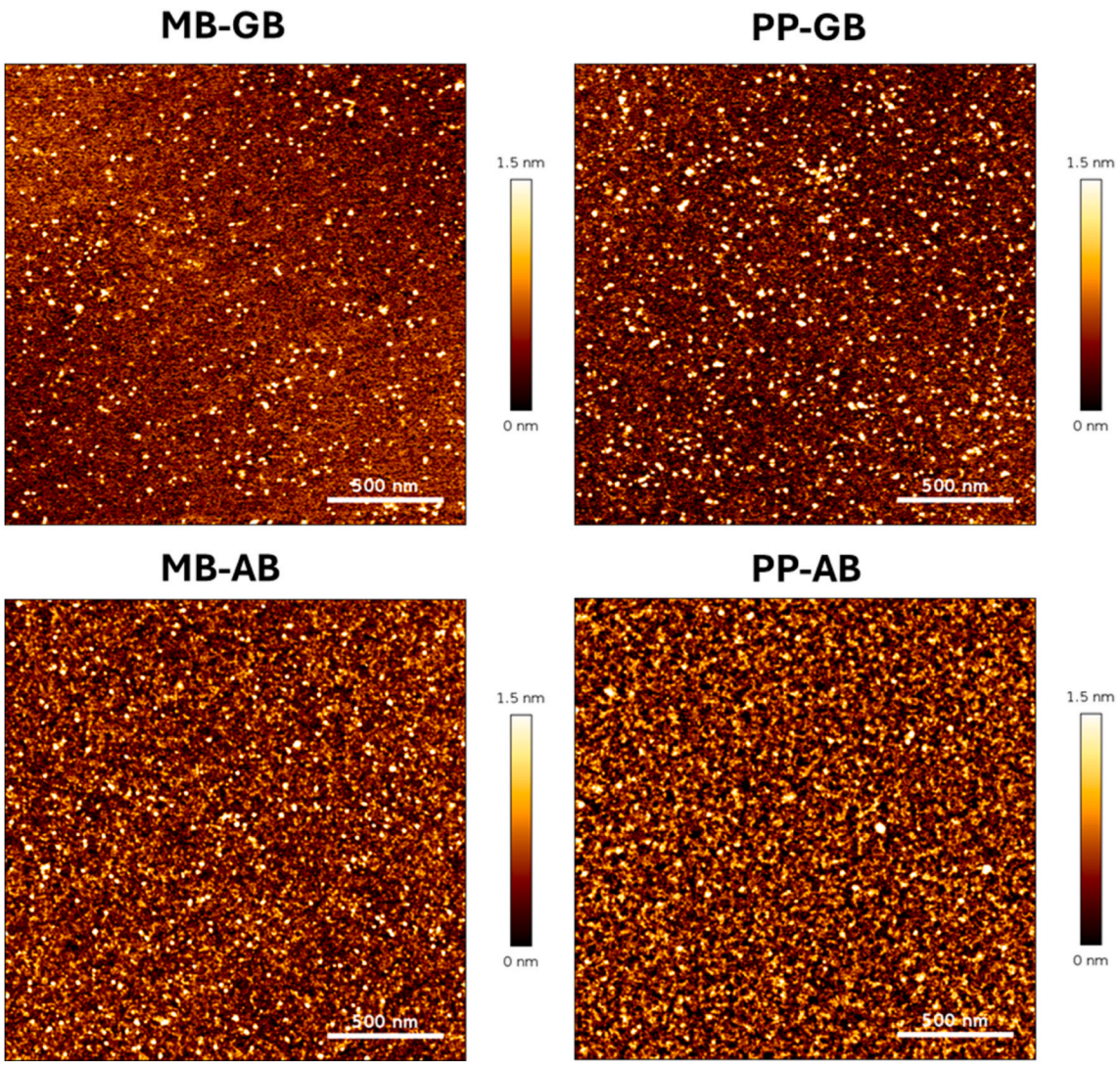


Fig. 6. AFM images of pulse protein-stabilized air-water interfaces, imaged from Langmuir-Blodgett films at surface pressures of 23 mN/m. The size of the images is 2 × 2 μm area with a resolution of 512 × 512 pixels.

longer average vessels length and lower lacunarity than that of PP-GB (Table S1). This indicated that MB-GB formed a denser and finer structure with higher surface coverage and lower heterogeneity compared to PP-GB-stabilized interface. PP-GB clearly formed a more open structure and tended to have higher extent of protein segregation than MB-GB. This structure indicates stronger in-plane interactions between the adsorbed proteins and could explain the higher resistance to density changes in dilatational rheology and higher stiffness in surface shear of the PP-GB-stabilized interface (Figs. 4B–5B). From the AFM images of AB-stabilized interfaces, it can be observed that PP-AB formed a slightly denser and finer structure compared to MB-AB. The PP-AB-stabilized interface had higher vessels area, higher number of junctions, higher junction density, longer average vessels length and lower lacunarity (Table S1). These values suggest that PP-AB had higher surface coverage and surface connectivity with a more homogenous structure. Despite forming a denser structure, the PP-AB-stabilized interface showed the lowest stiffness. The result suggests that although PP-AB adsorbs fast at the interface and has a high surface coverage, its structure does not have strong in-plane protein-protein interactions as evidenced by its low $E_{\tau 1L}$ and G_i' (Figs. 4A–5B). On the other hand, MB-AB formed a less dense structure with higher heterogeneity. It can be observed that the MB-AB film tended to have more protein segregation, and these protein clusters might contribute to its higher stiffness compared to that of the PP-AB film.

3.7. Foaming properties

The foam overrun of the four pulse protein fractions was evaluated by the whipping technique and calculated as the percentage increase in volume when air was incorporated into the liquid, compared to the initial liquid volume. From Fig. 7A, foam overruns of MB-GB, PP-GB, MB-AB, and PP-AB were 122%, 177%, 273, and 296%, respectively. A higher foam overrun of the AB fractions compared to the GB fractions was expected since the AB fractions adsorbed faster at air-water interfaces than the GB fractions. Similar to previous findings, pulse albumins (Lentil, faba bean, chickpea, mungbean, and pea) were reported to have better foam overrun compared to their GB fractions (Kornet et al., 2022; Shen et al., 2025; Yang et al., 2023). Interestingly, PP-GB foam had a significantly higher foam overrun than MB-GB foam, despite its initial adsorption at the air-water interface being slightly slower. A possible reason could be due to the differences in interfacial properties between these GB fractions. From dilatational rheology, the PP-GB-stabilized interface had a somewhat higher resistance to density changes ($E_{\tau 4}$), and a slightly higher stiffness in surface shear, which could help resist the immediate collapse of the air bubbles during foam formation. But differences in rheological parameters between these two

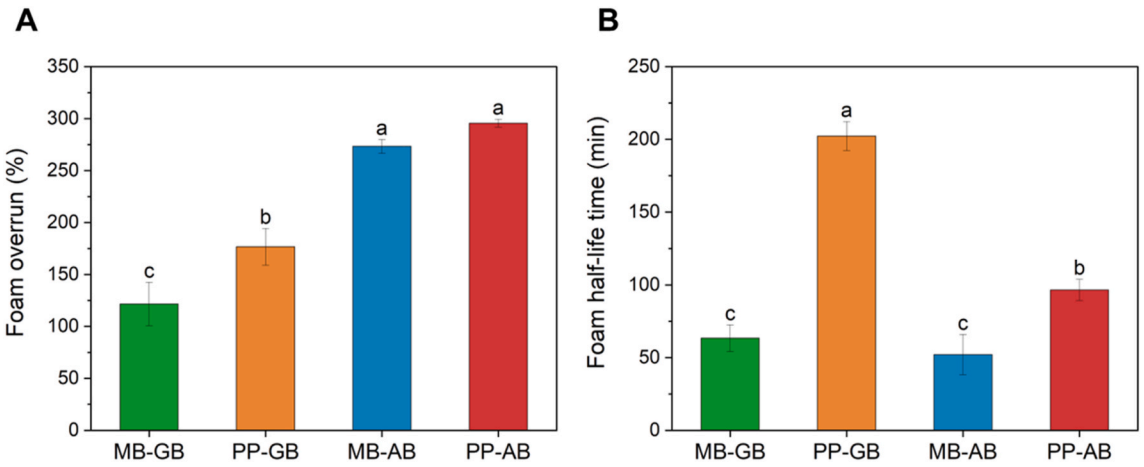


Fig. 7. **(A)** Foam overrun (%), and **(B)** foam half-life time (min) of the four pulse protein fractions: MB-GB (green), PP-GB (orange), MB-AB (blue), PP-AB (red). The different letters in the figure represent significantly different samples ($p < 0.05$).

samples are small, and other parameters (such as the disjoining pressure) may also be responsible for this difference in foam overrun.

Foam stability was assessed by sparging, by measuring the foam half-life time, which measured the time it took for the foam volume to decrease by half of its initial volume (Fig. 7B). In the literature, it is often reported that GB fractions of pulse proteins (pea, mung bean, lentil, faba bean, and chickpea) commonly have lower foam stability than their AB fractions (Kornet et al., 2022; Shen et al., 2025; Yang et al., 2023). This is mostly attributed to AB fractions forming foam with smaller bubble size and stiffer air-water interfaces, which can retard disproportionation and air bubble coalescence (Kornet et al., 2022). However, in our study, PP-GB foam exhibited superior foam stability compared to all other samples, with a foam half-life time of ~200 min. The PP-GB-stabilized interface showed strong network interaction in surface shear, and it had a high resistance to surface density changes. PP-GB also possessed a relatively high surface charge which can hinder the interfacial films of adjacent bubbles coming closer and collapsing. These properties of PP-GB together therefore slowed down disproportion and coalescence of air bubbles. The MB-AB-stabilized interface had the highest interfacial stiffness in both dilatation and shear, and thus we expected its foam to have high stability. However, MB-AB-stabilized foam was the least stable (foam half-life time of 52 min) and its stability was not significantly different from its GB fraction. Our result was inconsistent with a previous study of Yang et al. (2023) where MB-AB foam was reported to have superior foam stability, with a half-life time around 5 times higher than that of MB-GB foam. Possible reasons for this difference may be related to differences in experimental set up, for example the gas flow rate and the material of the porous frit. Another possible reason could be related to the material source. The cultivar of MB seed was reported to play an important role in the functional properties of its protein extracts (e.g., foaming capacity and foam stability) (Li et al., 2010). In AB fractions, owing to their faster adsorption, smaller air bubbles were generated during the initial stage of foam formation compared to GB fractions. In our study, the poor foam stability of MB-AB foam was possibly caused by the amount of protein being insufficient to cover all the interfaces in a short period of time (total foam sparging time was ~90–100s). This can lead to coalescence of air bubbles and induce foam instability. This destabilizing effect was less pronounced in PP-AB foam which was due to PP-AB adsorbing to the air-water interface faster than MB-AB as evident by a faster increase in surface pressure at 5–100s (Fig. 2A). MB-AB also had the most brittle interface in dilatation (i.e., the shortest LVE regime), and this may have also been a factor. Additionally, MB-AB-stabilized foam possibly had insufficient repulsive electrostatic interactions (in view of its low zeta potential, −9.8 mV) and steric repulsion resulting in a low disjoining pressure. This effect hence increased the possibility of liquid thin films draining and rupturing, leading to foam coarsening or collapse over time. Despite PP-AB having the weakest interfacial structure of all fractions, its foam was more stable than that of MB-AB and MB-GB. Due to the relatively high mobility of PP-AB on longer timescales, it possibly stabilized the air-water interface by the Marangoni effect. When liquid drainage occurred, the thin films were stretched and thinned, resulting in a surface tension gradient. This led to the adsorbed protein layers moving from the low-interfacial-tension toward the high-tension region of the liquid films, hence creating a flow of liquid to the thin part of the film (Damodaran, 2005). This process therefore helped slowing down the rate of liquid drainage. From this study, we found that PP proteins showed better foaming properties compared to MB proteins. The results suggested that type of pulse and protein fraction significantly affected foaming properties of pulse proteins. We also found that GB fractions do not always show inferior foam stability than AB fractions, as often observed in the literature.

4. Conclusion

In this study, we assessed the physico-chemical properties of MB and PP protein extracts prepared by wet conventional extraction and studied their interfacial properties at air-water interfaces and foaming properties. Albumin fractions from both MB and PP adsorbed at air-water interfaces faster than the GB fractions resulting in twofold higher foam overrun. This is due to their smaller particle size and lower surface charge. After adsorption, pulse protein-stabilized interfaces exhibited different responses in dilatational and shear deformation, especially in the nonlinear regimes. MB-AB formed an interfacial structure at the air-water interface with the highest stiffness, both in shear and dilatation, and it evidently had the strongest in-plane protein-protein interactions among all samples. Remarkably, PP-AB formed the weakest and most flexible interfacial structure. PP-AB-stabilized interfaces also showed a high dependence on frequency in shear deformation, displaying multimode Maxwell behavior. Therefore, it possibly stabilized the interface through the Marangoni effect rather than by imparting high stiffness to its film. In GB fractions, we observed that PP-GB-stabilized interfaces had stronger protein network interactions and higher resistance to density changes compared to MB-GB. These specific interfacial properties of PP-GB-stabilized interfaces resulted in higher foam overrun and foam stability than that of MB-GB. From the study of interfacial structures of these pulse proteins, all interfacial films showed heterogenous structures. We found that a denser structure was not directly related to a higher stiffness of interfacial structures. In foaming tests, PP proteins were found to have superior foaming ability compared to MB proteins at

the studied protein concentration (0.1%w/w). This demonstrated that PP proteins showed promising functionality as a plant-based ingredient in food applications based on foam. Further study may focus on varying protein concentration and pH for its effects on foaming properties. To utilize the potential of these pulse proteins, additional research could also explore the impact of other food ingredients (e.g., sugars and salts) on their functional properties. Overall, we found that both protein fraction and type of pulse play an important role in their interfacial and foaming properties. Even when there is high similarity in physico-chemical properties between the same protein fraction of two different pulses (i.e., surface charge and particle size), their behavior may be different. These differences could come from inherent molecular properties of the pulse proteins, such as post translational modifications. Therefore, proteomics analysis could be conducted in the future to provide more in-dept understanding such as more precise information on protein composition, their structures, and post-translational modifications. Lastly, it would also be interesting to further study the functional properties of these pulse proteins at the oil-water interface to explore their potential applications in emulsion-based foods.

CRediT authorship contribution statement

Ployfon Boonkor: Writing – original draft, Visualization, Validation, Methodology, Investigation, Conceptualization. **Jasper Landman:** Writing – review & editing, Supervision, Conceptualization. **Chaiwut Gamonpilas:** Writing – review & editing, Supervision, Conceptualization. **Leonard M.C. Sagis:** Writing – review & editing, Supervision, Methodology, Funding acquisition, Conceptualization.

Declaration of competing interest

The authors have declared that no competing interest exist.

Acknowledgements

This research received funding from the Dutch Research Council (NWO) in the framework of the Southeast Asia-Europe Joint Funding Scheme Call for Proposals (SEA-EU JFS CALL), and funding support from the NSRF via Program Management Unit for Human Resources & Institutional Development, Research and Innovation [grant number B48G660107], Thailand.

Appendix A. Supplementary data

Supplementary data to this article can be found online at https://doi.org/10.1016/j.foodhyd.2026.112681.

Data availability

Data will be made available on request.

References

Anwar, F., Latif, S., Przybylski, R., Sultana, B., & Ashraf, M. (2007). Chemical composition and antioxidant activity of seeds of different cultivars of mungbean. *Journal of Food Science, 72*(7), S503–S510. https://doi.org/10.1111/j.1750-3841.2007.00462.x

Bernklau, I., Lucas, L., Jekle, M., & Becker, T. (2016). Protein network analysis — A new approach for quantifying wheat dough microstructure. *Food Research International, 89*, 812–819. https://doi.org/10.1016/j.foodres.2016.10.012

Beverung, C. J., Radke, C. J., & Blanch, H. W. (1999). Protein adsorption at the oil/water interface: Characterization of adsorption kinetics by dynamic interfacial tension measurements. *Biophysical Chemistry, 81*(1), 59–80. https://doi.org/10.1016/S0301-4622(99)00082-4

Boye, J., Zare, F., & Pletch, A. (2010). Pulse proteins: Processing, characterization, functional properties and applications in food and feed. *Food Research International, 43*(2), 414–431. https://doi.org/10.1016/j.foodres.2009.09.003

Brishti, F. H., Zarei, M., Muhammad, S. K. S., Rashedi, I. F. M., Shukri, R., & Saari, N. (2017). *Evaluation of the functional properties of mung bean protein isolate for development of textured vegetable protein*.

Chibbar, R. N., Ambigaipalan, P., & Hoover, R. (2010). REVIEW: Molecular diversity in pulse seed starch and complex carbohydrates and its role in human nutrition and health. *Cereal Chemistry, 87*(4), 342–352. https://doi.org/10.1094/CCHEM-87-4-0342

Chutinara, C., Sagis, L. M. C., & Landman, J. (2024). Interfacial rheological properties of pepsin-hydrolyzed lentil protein isolate at oil-water interfaces. *Food Hydrocolloids, 155*, Article 110201. https://doi.org/10.1016/j.foodhyd.2024.110201

Damodaran, S. (2005). Protein stabilization of emulsions and foams. *Journal of Food Science, 70*(3), R54–R66. https://doi.org/10.1111/j.1365-2621.2005.tb07150.x

de Groot, A., Yang, J., & Sagis, L. M. C. (2023). Surface stress decomposition in large amplitude oscillatory interfacial dilatation of complex interfaces. *Journal of Colloid and Interface Science, 638*, 569–581. https://doi.org/10.1016/j.jcis.2023.02.007

Du, M., Xie, J., Gong, B., Xu, X., Tang, W., Li, X., Li, C., & Xie, M. (2018). Extraction, physicochemical characteristics and functional properties of mung bean protein. *Food Hydrocolloids, 76*, 131–140. https://doi.org/10.1016/j.foodhyd.2017.01.003

Etzbach, L., Gola, S., Küllmer, F., Acir, I.-H., Wohlt, D., Ignatzy, L. M., Bader-Mittermaier, S., & Schweiggert-Weisz, U. (2024). Opportunities and challenges of plant proteins as functional ingredients for food production. *Proceedings of the National Academy of Sciences, 121*(50), Article e2319019121. https://doi.org/10.1073/pnas.2319019121

Ewoldt, R., Hosoi, A., & McKinley, G. (2008). New measures for characterizing nonlinear viscoelasticity in large amplitude oscillatory shear. *Journal of Rheology - J RHEOL, 52*. https://doi.org/10.1122/1.2970095

Ho, T. M., Bhandari, B. R., & Bansal, N. (2022). Functionality of bovine milk proteins and other factors in foaming properties of milk: A review. *Critical Reviews in Food Science and Nutrition, 62*(17), 4800–4820. https://doi.org/10.1080/10408398.2021.1879002

Huang, Z., Li, Y., Fan, M., Qian, H., & Wang, L. (2024). Recent advances in mung bean protein: From structure, function to application. *International Journal of Biological Macromolecules, 273*, Article 133210. https://doi.org/10.1016/j.ijbiomac.2024.133210

Ismail, B. P., Senaratne-Lenagala, L., Stube, A., & Brackenridge, A. (2020). Protein demand: Review of plant and animal proteins used in alternative protein product development and production. *Animal Frontiers, 10*(4), 53–63. https://doi.org/10.1093/af/vfaa040

Joyner, H. S. (2021). Nonlinear (Large-Amplitude oscillatory shear) rheological properties and their impact on food processing and quality. *Annual Review of Food Science and Technology, 12*, 591–609. https://doi.org/10.1146/annurev-food-061220-100714, 12, 2021.

Kornet, R., Yang, J., Venema, P., van der Linden, E., & Sagis, L. M. C. (2022). Optimizing pea protein fractionation to yield protein fractions with a high foaming and emulsifying capacity. *Food Hydrocolloids, 126*, Article 107456. https://doi.org/10.1016/j.foodhyd.2021.107456

Krishna, T. G., & Bhatia, C. R. (1985). Vicilin from cajanus cajan seeds. *Phytochemistry, 24*(10), 2201–2203. https://doi.org/10.1016/S0031-9422(00)83010-1

Li, W., Shu, C., Yan, S., & Shen, Q. (2010). Characteristics of sixteen mung bean cultivars and their protein isolates. *International Journal of Food Science and Technology, 45*(6), 1205–1211. https://doi.org/10.1111/j.1365-2621.2010.02259.x

Locali-Pereira, A. R., Boire, A., Berton-Carabin, C., Taboga, S. R., Solé-Jamault, V., & Nicoletti, V. R. (2023). Pigeon Pea, an emerging source of plant-based proteins. *ACS Food Science & Technology, 3*(11), 1777–1799. https://doi.org/10.1021/acsfoodscitech.3c00268

Locali-Pereira, A., Solé, V., Davy, J., Cherkaoui, M., Rogniaux, H., Mameri, H., Le Gall, S., Beaumal, V., Rabesona, H., Laurent, S., Nicoletti, V., Berton-Carabin, C., & Boire, A. (2025). Large-scale chromatography for the isolation of 7S globulin enriched fraction from pigeon pea seeds. *Journal of Agricultural and Food Chemistry, 73*. https://doi.org/10.1021/acs.jafc.5c01681

Lucassen, J., & Van Den Tempel, M. (1972). Dynamic measurements of dilational properties of a liquid interface. *Chemical Engineering Science, 27*(6), 1283–1291. https://doi.org/10.1016/0009-2509(72)80104-0

Ma, X., Habibi, M., & Sagis, L. M. C. (2024). Interfacial and foaming properties of soluble lupin protein isolates: Effect of pH. *Food Hydrocolloids, 155*, Article 110228. https://doi.org/10.1016/j.foodhyd.2024.110228

Mendoza, E. M. T., Adachi, M., Bernardo, A. E. N., & Utsumi, S. (2001). Mungbean [Vigna radiata (L.) Wilczek] Globulins: Purification and Characterization. *Journal of Agricultural and Food Chemistry, 49*(3), 1552–1558. https://doi.org/10.1021/jf001041h

Oomah, B. D., Patras, A., Rawson, A., Singh, N., & Compos-Vega, R. (2011). 2 - Chemistry of pulses. In B. K. Tiwari, A. Gowen, & B. McKenna (Eds.), *Pulse foods* (pp. 9–55). Academic Press. https://doi.org/10.1016/B978-0-12-382018-1.00002-2.

Oshodi, A. A., & Ekperigin, M. M. (1989). Functional properties of pigeon pea (Cajanus cajan) flour. *Food Chemistry, 34*(3), 187–191. https://doi.org/10.1016/0308-8146(89)90139-8

Phillips, L. G., Whitehead, D. M., & Kinsella, J. (1994). Chapter 6 - Protein-Stabilized foams. In L. G. Phillips, D. M. Whitehead, & J. Kinsella (Eds.), *Structure–function properties of food proteins* (pp. 131–152). Academic Press. https://doi.org/10.1016/B978-0-12-554360-6.50011-5.

Pivard, S., Jacomine, L., Kratz, F. S., Foussat, C., Lamps, J. P., Legros, M., Boulmedais, F., Kierfeld, J., Schosseler, F., & Drenckhan, W. (2024). Interfacial rheology of linearly growing polyelectrolyte multilayers at the water-air interface: From liquid to solid viscoelasticity. *Soft Matter, 20*(6), 1347–1360. https://doi.org/10.1039/d3sm01161e

Prakash, S., Gaiani, C., & Bhandari, B. R. (2023). Chapter 1 - Plant-Based food as a sustainable source of food for the future. In S. Prakash, B. R. Bhandari, & C. Gaiani (Eds.), *Engineering plant-based food systems* (pp. 1–12). Academic Press. https://doi.org/10.1016/B978-0-323-89842-3.00005-1.

Pratap, A., Gupta, S., Rathore, M., Basavaraja, T., Singh, C. M., Prajapati, U., Singh, P., Singh, Y., & Kumari, G. (2021). Chapter 1 - Mungbean. In A. Pratap, & S. Gupta (Eds.), *The beans and the peas* (pp. 1–32). Woodhead Publishing. https://doi.org/10.1016/B978-0-12-821450-3.00009-3.

Rodríguez Patino, J. M., Carrera Sánchez, C., & Rodríguez Niño, M. R. (2008). Implications of interfacial characteristics of food foaming agents in foam formulations. *Advances in Colloid and Interface Science, 140*(2), 95–113. https://doi.org/10.1016/j.cis.2007.12.007

Sagis, L. M. C., & Fischer, P. (2014). Nonlinear rheology of complex fluid–fluid interfaces. *Current Opinion in Colloid & Interface Science, 19*(6), 520–529. https://doi.org/10.1016/j.cocis.2014.09.003

Sagis, L. M. C., & Yang, J. (2022). Protein-stabilized interfaces in multiphase food: Comparing structure-function relations of plant-based and animal-based proteins. *Current Opinion in Food Science, 43*, 53–60. https://doi.org/10.1016/j.cofs.2021.11.003

Shen, P., Ha, S. M. L., Peng, J., Landman, J., & Sagis, L. M. C. (2025). Role of pulse globulins and albumins in air-water interface and foam stabilization. *Food Hydrocolloids, 160*, Article 110792. https://doi.org/10.1016/j.foodhyd.2024.110792

Shen, P., Peng, J., Sagis, L. M. C., & Landman, J. (2024). Air-water interface properties and foam stabilization by mildly extracted lentil protein. *Food Hydrocolloids, 147*, Article 109342. https://doi.org/10.1016/j.foodhyd.2023.109342

Syed, R., Ding, H. H., Hui, D., & Wu, Y. (2022). Physicochemical and functional properties of pigeon pea (Cajanus cajan) protein and non-starch polysaccharides. *Bioactive Carbohydrates and Dietary Fibre, 28*, Article 100317. https://doi.org/10.1016/j.bcdf.2022.100317

Tang, X., Shen, Y., Zhang, Y., Schilling, M. W., & Li, Y. (2021). Parallel comparison of functional and physicochemical properties of common pulse proteins. *LWT, 146*, Article 111594. https://doi.org/10.1016/j.lwt.2021.111594

Tripathi, A., Iswarya, V., Rawson, A., Singh, N., Oomah, B. D., & Patras, A. (2021). Chapter 3 - Chemistry of pulses—macronutrients. In B. K. Tiwari, A. Gowen, & B. McKenna (Eds.), *Pulse foods* (2nd ed., pp. 31–59). Academic Press. https://doi.org/10.1016/B978-0-12-818184-3.00003-9.

Walstra, P. (2003). *Physical chemistry of foods*. Marcel Dekker.

Yang, J., de Wit, A., Diedericks, C. F., Venema, P., van der Linden, E., & Sagis, L. M. C. (2022). Foaming and emulsifying properties of extensively and mildly extracted Bambara groundnut proteins: A comparison of legumin, vicilin and albumin protein. *Food Hydrocolloids, 123*, Article 107190. https://doi.org/10.1016/j.foodhyd.2021.107190

Yang, J., Yang, Q., Waterink, B., Venema, P., de Vries, R., & Sagis, L. M. C. (2023). Physical, interfacial and foaming properties of different mung bean protein fractions. *Food Hydrocolloids, 143*, Article 108885. https://doi.org/10.1016/j.foodhyd.2023.108885

Yi-Shen, Z., Shuai, S., & FitzGerald, R. (2018). Mung bean proteins and peptides: Nutritional, functional and bioactive properties. *Food & Nutrition Research, 62*. https://doi.org/10.29219/fnr.v62.1290

Zhao, Q., Ding, L., Xia, M., Huang, X., Isobe, K., Handa, A., & Cai, Z. (2021). Role of lysozyme on liquid egg white foaming properties: Interface behavior, physicochemical characteristics and protein structure. *Food Hydrocolloids, 120*, Article 106876. https://doi.org/10.1016/j.foodhyd.2021.106876

Zudaire, E., Gambardella, L., Kurcz, C., & Vermeren, S. (2011). A computational tool for quantitative analysis of vascular networks. *PLoS One, 6*(11), Article e27385. https://doi.org/10.1371/journal.pone.0027385